# Chapter 5: Quantum Monte Carlo Calculations with Multi-Reference Trial Wave Functions

HEINZ-JÜRGEN FLAD
*Max-Planck-Institut für Physik komplexer Systeme*
*(Außenstelle Stuttgart) 70569 Stuttgart, Heisenbergstr. 1, Germany*

MICHEL CAFFAREL and ANDREAS SAVIN
*Laboratoire de Chimie Théorique*
*(CNRS, UPR 271), Université Pierre et Marie Curie,*
*Tour 22, 4 Place Jussieu, 75252 Paris, Cedex 05, France*

## 1. Introduction.

Quantum Monte Carlo (QMC) methods offer a possibility for very accurate calculations of correlation energies for atoms and molecules [1]. An important aspect of these calculations is that one has to take care of the change of sign of the wave function during the random walk in configuration space. Several exact solutions to this problem have been proposed. We will just mention the method of correlated walkers of Arnow *et al.* [2] (see also [3]), the released-node method of Ceperley and Alder [4], the projection method of Caffarel and Claverie [5], and the method of Anderson *et al.* [6]. Despite the great success of these kinds of methods in some selected cases, its possible range of application still remains limited. Twenty years ago Anderson suggested a very simple and efficient approximation, the so-called fixed-node approximation [7]. It permits an exact stochastic solution of the Schrödinger equation within a supplementary boundary condition. This boundary condition is given by the nodal structure of a trial wave function and the stochastic solution is forced to have the same nodes. The resulting energies are upper bounds of the exact ground state energies (see e.g. [8] for a recent review). The importance of this approximate scheme in QMC calculations is due to its robustness and asymptotic stability. Most of the QMC applications for atoms and molecules published in the literature have been carried out within the fixed-node approximation. At present it is unrivaled for calculations including heavy elements [9, 10, 11, 12]. Moreover the fixed-node approximation is the starting point for exact released-node calculations [4].

The crucial point of the fixed-node approximation is the selection of the trial wave function which defines the nodal structure. If the approximate nodes are close

to the exact ones, it is possible to get very accurate results for a variety of physical properties, like bond energies, excitation and ionization energies and electron affinities, which are often rather sensitive to electron correlation. Unfortunately, the nodal structure of many-electron wave functions is still rather mysterious. Apart from symmetry restrictions, a general $N$-electron wave function depends on the complete set of the $3N$ variables of the configuration space. The nodes are represented by a $(3N-1)$-dimensional hypersurface in this space. It has been demonstrated by Ceperley [13] that the exact ground state wave functions satisfy what he called the tiling property, which means that there exits only one type of nodal cell and all others can be obtained by permuting the particles in a suitable way. The arguments given by Ceperley can in general not be extended to approximate wave functions because the wave function has to be an eigenfunction of a Hamiltonian with local potential. The local potential may have at most a weak singularity at the nodes. It is in general not possible to determine the structure of the nodes from symmetry considerations which contain permutational and point group symmetries [14]. This can be seen by counting the number of constraints imposed on the configuration space. Due to permutational symmetry the wave function vanishes if two electrons with equal spin occupy the same part of space. The three constraints $\vec{r}_i = \vec{r}_j$ belonging to it generate a $(3N-3)$-dimensional hypersurface, which represents only a subset of the complete nodal hypersurface.

An appropriate choice for the trial wave function has therefore to take into account not only symmetry requirements but also the electron interactions. Usually the nodes of Hartree-Fock (HF) wave functions are used for the fixed-node approximation. These trial wave functions are solutions of nonlocal mean-field equations but their structure is very close to solutions of Kohn-Sham equations with local exchange-correlation potential. Therefore they will probably satisfy the tiling property [13]. In some cases the HF wave function yields only a very poor description of the ground state due to accidental near degeneracies. Extension of the wave function by inclusion of the configurations which are energetically close to the HF configuration overcomes this difficulty. A well-known example is the Be atom which has been studied by Harrison and Handy [15]. In this case we have a strong near-degeneracy between two configurations with $1s^2 2s^2$ and $1s^2 2p^2$ occupancies. The fixed-node correlation energy can be improved by 10 % in going from HF to the two-configuration self-consistent-field wave function. Obviously it is in general straightforward to improve the HF wave function in a systematic way by adding selected configurations. This procedure includes some arbitrariness because the magnitude of the coefficients decreases quite uniformly.

In the remaining part of the paper we will discuss the effects of different types of configurations on the fixed-node energies of the atoms B to F. Starting with conventional complete active space self-consistent field (CASSCF) calculations, we have selected the dominant configuration state functions (CSFs). These have been added successively to the trial wave function, making it feasible to study the impact of

different types of excitations on the nodal structure. Unfortunately, it is not readily possible to conclude from the contribution to the total energy of a CSF its importance for the nodes.

At the end of this section we will briefly discuss possible methods to obtain trial wave functions from standard methods in quantum chemistry. Due to the fact, that one has to calculate the value of the wave function and its derivatives, only a small number of configurations can be taken into account. To calculate such wave functions, the multi-configuration self-consistent field (MCSCF) method seems to be most appropriate. The orbitals and coefficients are optimized simultaneously with respect to the energy but this does not mean, that they are also optimal with respect to the nodes. Therefore one can think to replace the MCSCF orbitals by other types of orbitals like natural or Brueckner orbitals. The first possibility has been suggested by Grossman and Mitáš in the case of silicon clusters [16]. For these systems they obtained a slight improvement of their results by using natural orbitals in a single determinant wave function.

## 2. Generation of CSFs for QMC calculations.

QMC methods which make use of trial wave functions differ in an essential point from other methods usually applied in quantum chemistry. In contrast to most other methods, QMC works in a spin-free formalism and it is necessary to calculate the value of the trial wave function explicitly. This can raise difficulties if one wants to use the outputs of atomic or molecular program packages to generate the trial wave functions, at least for open shell configurations. In this section we give a brief description how to construct spin-free trial wave functions for configurations with more than one open shell. Spin-free formalisms are currently rarely used in quantum chemistry, nevertheless their theory is well developed (see e.g. the book of Pauncz [17]). We will choose an approach which is appropriate for the peculiarities of QMC calculations.

Due to the fact, that the Hamiltonian is symmetric with respect to permutations of electrons, it is possible to classify the eigenfunctions with respect to the irreducible representations of the symmetric group [18]. Here we consider only the nonrelativistic case, where the Hamiltonian contains no spin-dependent interactions. Therefore the eigenfunctions depend only on the spatial coordinates. The irreducible representations generated by spatial eigenfunctions can be characterized by Young frames with at most two columns. The number of boxes $N$ is equal to the number of electrons. The difference between the number of boxes in the left and right columns determines the total spin of the wave function and is equal to $2S$ (see Figure 1). Distributing the numbers $1, \ldots, N$ among the boxes of the Young frame, one gets a Young tableau, which can be viewed as an element of the group algebra. Each element of the group algebra can be represented by a linear combination of elements of the symmetric group $S_N$. A Young tableau $Y$ can be generated from two subgroups of the symmet-

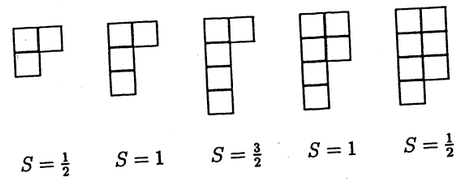

$S=\frac{1}{2}$ $S=1$ $S=\frac{3}{2}$ $S=1$ $S=\frac{1}{2}$

Figure 1: Young frames for irreducible representations of the symmetric group, which correspond to the valence part of the wave functions considered in this paper. The total spin is determined by the number of rows with only a single box.

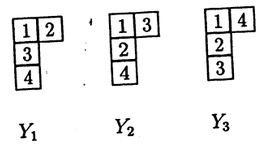


$Y_1$ $Y_2$ $Y_3$

Figure 2: Standard Young tableaux for the second Young frame in Figure 1.

ric group. The subgroups $P_Y(S_N)$, and $N_Y(S_N)$, contain all elements of $S_N$ which permute numbers only within the rows and columns of $Y$, respectively. From these two subgroups one gets the following two elements of the group algebra

$$\hat{P}_Y = \sum_i \hat{g}_i, \quad \hat{g}_i \in P_Y(S_N); \qquad \hat{N}_Y = \sum_i (-1)^{|g_i|}\hat{g}_i, \quad \hat{g}_i \in N_Y(S_N) \tag{1}$$

where $|g_i|$ is the number of single permutations in which the element $\hat{g}_i$ can be decomposed. The sum is over all elements of the corresponding subgroup. Both elements of the group algebra can act as operators on arbitrary functions $\Phi(x_1, x_2, \ldots, x_N)$,

$$\hat{P}_Y\Phi(x_1, x_2, \ldots, x_N) = \sum_i \hat{g}_i\Phi(x_1, x_2, \ldots, x_N) \tag{2}$$

$$\hat{N}_Y\Phi(x_1, x_2, \ldots, x_N) = \sum_i (-1)^{|g_i|}\hat{g}_i\Phi(x_1, x_2, \ldots, x_N). \tag{3}$$

The function $\hat{P}_Y\Phi$ ($\hat{N}_Y\Phi$) is symmetric (antisymmetric) with respect to variables within a common row (column). The product of both operators

$$\hat{E}_Y = \hat{N}_Y\hat{P}_Y \tag{4}$$

can be associated with the Young tableau $Y$, whereby the properties of $\hat{E}_Y$ are completely determined through the assignment of the numbers and the shape of the Young frame. From a given Young frame one can generate several different Young tableaux $Y_i$. Usually it is sufficient to consider only standard Young tableaux, which means that the numbers in each row and column are arranged in ascending order from left to right and from top to bottom (see Figure 2). Taking an arbitrary standard Young tableau $Y_1$ as a reference, we can define operators

$$\hat{E}_{Y_i} = \hat{N}_{Y_i} \hat{P}_{Y_i} \hat{g}_{i1} \tag{5}$$

whereby $\hat{g}_{i1}$ represents the permutation which transforms $Y_1$ to $Y_i$. The operators $\hat{E}_{Y_i}$ constitute a set which is not linearly independent. A set of independent operators can be obtained from the standard Young tableaux. By applying these operators to an arbitrary function $f(x_1, x_2, \ldots, x_N)$ a $D$ dimensional irreducible representation of $S(N)$ is generated, where $D$ is the number of standard Young tableaux.

$$\Phi_i(x_1, x_2, \ldots, x_N) = \hat{E}_{Y_i} \Phi(x_1, x_2, \ldots, x_N) \tag{6}$$

The functions $\Phi_i(x_1, x_2, \ldots, x_N)$ can be viewed as spatial parts of fermionic wave functions. For fermions the total wave function has to be antisymmetric with respect to the simultaneous permutation of both spatial and spin coordinates of any pair of electrons. Based on previous work of Fock [19] (see e.g. the book of Hamermesh [20] for a brief exposition), Drukarev [21] and Demkov [22] demonstrated that the total wave function can be represented by a sum of products of spatial functions $\Phi_i$ and spin functions $\Xi_i$

$$\Psi[(\vec{r}\vec{\sigma})_1, \ldots, (\vec{r}\vec{\sigma})_n] = C_N \sum_i (-1)^{|g_{i1}|} \Phi_i(\vec{r}_1, \ldots, \vec{r}_n)\, \Xi_i(\vec{\sigma}_1, \ldots, \vec{\sigma}_n)\,. \tag{7}$$

The index i runs over all possible Young tableaux. The spin functions $\Xi_i(\vec{\sigma}_1, \ldots, \vec{\sigma}_n)$ appearing in Eq. 7, can be generated from a Young tableau $Y_i^T$ with at most two rows, which is obtained from $Y_i$ by converting columns into rows [18] and reversing the order of the operators in Eq. 4. The generating spin function $\Xi$ is conveniently chosen to be a product of the form

$$\Xi(1, \ldots, n) = \prod_{i=1}^{\frac{N+2S}{2}} \alpha(k_i) \prod_{i=1}^{\frac{N-2S}{2}} \beta(l_i) \tag{8}$$

which assures that the $\Xi_i$ are eigenfunctions of $\hat{S}^2$ and $\hat{S}_z$,with $S_z = S$. The indices $k_i$ ($l_i$) refer to the numbers in the first (second) row of $Y_i^T$. It can be shown [17] that the following relation

$$\frac{\langle \Psi \mid \hat{H} \mid \Psi \rangle}{\langle \Psi \mid \Psi \rangle} = \frac{\langle \Phi_i \mid \hat{H} \mid \Phi_i \rangle}{\langle \Phi_i \mid \Phi_i \rangle} \quad \forall i \tag{9}$$

applies to the expectation value of the energy. Therefore it is sufficient to consider only one spatial wave function $\Phi_i$. It is obvious, that the $\Phi_i$ are all equivalent due to the fact that the Hamiltonian is invariant with respect to permutations.

In addition to permutational symmetries one has to take into account spatial symmetry requirements. Atomic wave functions are characterized according to their spin ($S$) and angular momentum ($L$) eigenvalues . For a nonrelativistic Hamiltonian without spin-orbit coupling $L, S$ are good quantum numbers. It is usually possible to construct different angular momentum eigenfunctions for given $L$ value and occupation number $n$ of the shell. Within each $l^n$ shell different coupling schemes can be characterized by their angular momentum $L_{l^n}$ within the shell and a seniority quantum number $\sigma$ [23], which specifies the number of electron pairs coupled to zero angular momentum. The final eigenfunction can be obtained by coupling eigenfunctions $\phi(l^n, L_{l^n}, \sigma)$ of different shells in a convenient way. Programs like GENCL which is a part of the MCHF atomic-structure package of Froese Fischer [24] can be used to generate a list of possible coupling schemes. The explicit construction of eigenfunctions in a form suitable for QMC calculations is straightforward. Starting from one-particle eigenfunctions $Y_{lm}$ within each shell, it is a simple genealogical construction using the standard methods for angular momentum coupling.

$$\begin{aligned} \phi^{l^2}_{L'0}(1,2) &= \sum_m \langle lm, l(-m) \mid L'0\rangle\, Y_{lm}(1) Y_{l(-m)}(2) \\ \phi^{l^3}_{L''0}(1,2,3) &= \sum_{M'} \langle L'M', l(-M') \mid L''0\rangle\, \phi^{l^2}_{L'M'}(1,2) Y_{l(-M')}(3) \\ &\vdots \end{aligned} \tag{10}$$

Here $\langle l_1 m_1, l_2 m_2 \mid LM\rangle$ are Clebsch-Gordan coefficients which can be easily obtained from the corresponding 3j-symbols [23]. Only eigenfunctions with $M = 0$ have been calculated in this way. The other $M$ values have been obtained by repeated application of the ladder-operators.

$$\hat{L}_{\pm}\phi_{L'M'}(1,2,\ldots,n) = \sqrt{L'(L'+1) - M'(M'\pm 1)}\;\phi_{L'(M'\pm 1)}(1,2,\ldots,n) \tag{11}$$

It is convenient to chose $M = 0$ because it gives a real function, just as well one can take a real linear combination of $\phi_{LM}$ and $\phi_{L(-M)}$. The $Y_{l_i m_i}(i)$ are still complex and have to be replaced by real spherical harmonics $Z_{l_i m_i}(i)$. The final angular momentum eigenfunction $\phi_{L0}$ is a linear combination of products of one-particle functions.

$$\phi_{L0}(1,2,\ldots,N) = \sum_{m_1 \ldots m_N} C^{L0}_{l_1 m_1 \ldots l_N m_N} \prod_{i=1}^{N} Z_{l_i m_i}(i) \tag{12}$$

If the eigenfunction includes open shells with equal $l$ quantum number, it is necessary to distinguish the $Z_{lm}$ which belong to different shells.

Up to now $\phi_{L0}$ does not represent a fermionic wave function because it does not show the correct behavior with respect to permutations of particles. In order to

obtain the spatial part of the trial wave function one has to apply the operator $\hat{E}_Y$ from an arbitrary Young tableau to $\phi_{L0}$ (see Eq. 6). However this is not sufficient to get all the required CSFs. The CSFs differ not only in the manner in which the angular momentum of the spatial parts are coupled, they can also differ in their spin coupling scheme (see Appendix A). This is related to the fact, that we can get different functions by interchanging the order of the variables in $\phi_{L0}$. In order to obtain all possible spin couplings it is sufficient to pick out a standard Young tableau $Y_1$ and to determine all the permutations $\hat{g}_{1i}$ which transform the standard Young tableaux $Y_i$ to $Y_1$. The spatial trial wave functions belonging to different spin couplings can then be generated using the operators $\hat{E}_{Y_1}\hat{g}_{1i}$, which act on the angular momentum eigenfunctions.

$$\Phi^i_{L0}(\vec{r}_1,\vec{r}_2,\ldots,\vec{r}_N) = \hat{E}_{Y_1}\ \hat{g}_{1i}\ \phi_{L0}(\vec{r}_1,\vec{r}_2,\ldots,\vec{r}_N) \tag{13}$$

The operator $\hat{E}_{Y_1}$ symmetrizes the variables within the rows and thereafter it antisymmetrizes the variables within the columns. Applying it to a product of one-particle functions as it appears in Eq. 12, results in a sum of products of two determinants.

$$\Phi^i_{L0} = \sum_{l_1 m_1 \ldots l_N m_N} \overline{C}^{L0}_{l_1 m_1 \ldots l_N m_N}\ |\ Z_{l_1 m_1}\ldots Z_{l_\alpha m_\alpha}\ |\ |\ Z_{l_{\alpha+1} m_{\alpha+1}}\ldots Z_{l_N m_N}\ | \tag{14}$$

In each product the two determinants represent electrons with $\alpha$ and $\beta$ spins, respectively. Closed shells which have not been considered so far can be easily incorporated by inserting their orbitals in both determinants. This form of the trial wave function enables an efficient evaluation of the local energy in QMC calculations [1]. The $\Phi^i_{L0}$ are not necessarily orthogonal nor linearly independent, depending on the system under consideration. Eliminating linear dependencies yields a set of basis functions $\Phi^i_{L0}$ which constitute a vector space $V(L)$. Finally it is necessary to identify the specific spin couplings in $V(L)$. This can be done by a Schmidt-orthogonalization of the remaining $\Phi^i_{L0}$ and performing a convenient orthogonal transformation

$$\overline{\Phi}^i_{L0}(\vec{r}_1,\vec{r}_2,\ldots,\vec{r}_N) = \sum_j \Gamma_{ij}\ \Phi^j_{L0}(\vec{r}_1,\vec{r}_2,\ldots,\vec{r}_N)\,. \tag{15}$$

For the systems under consideration it is straightforward to determine the matrix elements $\Gamma_{ij}$ by inspection of the determinants which constitute the $\Phi^i_{L0}$. There are at most two or three different spin couplings between open shells for each $\phi_{L0}$ and some products possess typical distributions of the $Z_{lm}$ on the determinants which are unique for a specific spin coupling. Requiring $\Gamma$ to decouple these determinants determines the $\Gamma_{ij}$ uniquely (see Appendix B). After we have established a one to one correspondence between the CSFs from a conventional *ab initio* calculation and the spin-free CSFs used in QMC calculations, it remains to fix the sign of their coefficients in the trial wave function. If the number of CSFs is small it takes usually less effort to perform a few short VMC calculations to fix the signs. In some cases where

an occupation gives rise to several CSFs, it is possible to determine their relative signs from conventional *ab initio* calculations. Usually the CSFs have some common determinants. We have performed MCSCF calculations in a determinant basis using the MOLPRO program of Werner and Knowles [25, 26]. From the absolute values of the coefficients of the determinants which are common to several CSFs one can easily obtain their relative signs. The absolute sign has been again determined from VMC calculations. Further details are given in Appendices A and B.

## 3. Selection of the dominant CSFs for the ground states of the atoms B to F.

The expansion of a wave function as a sum of determinants is the most common method in quantum chemistry to calculate electron correlation. The determinants are usually composed of orbitals taken from a preceding calculation. For a convenient set of orbitals, like natural or MCSCF orbitals, the convergence of the energy is very fast at the beginning but slows down considerably with increasing expansion length [27]. The deterioration of the convergence results from short range correlations which are poorly described by linear combinations of determinants [28]. We have restricted ourselves to the most important CSFs. Single excitations can be neglected due to the generalized Brillouin theorem.

The HF configurations for B to F possess a $2s^2 2p^n$ occupation in the valence shells. Within the valence space, a double excitation $2s^2 2p^n \rightarrow 2p^{n+2}$ is possible for B and C, otherwise no such excitations can occur. Thereafter a $2s$ electron can be put into the $3d$ shell. The resulting $2s^1 2p^n 3d^1$ configurations are not single excitations due to regroupings within the $2p$ shell. This type of CSF can be generated for the whole row B to F. Further important CSFs can be obtained from $2s^1 3s^1 2p^{n-1} 3p^1$ and $2s^2 2p^{n-2} 3p^2$ occupations. We have performed CASSCF calculations for these occupations using the MCHF program of Froese Fischer [24], in order to determine their contributions to the correlation energy. This means that we have included all possible CSFs within a given occupation. The results are shown in Figure 3, which shows the contributions of the most important occupations for each atom. For the $^2P$ ground state of B the most significant improvement can be achieved by adding the $2p^3$ configuration. Similar improvement can be obtained by including in addition the two CSFs with $2s^1 2p^1 3d^1$ occupation. All other occupations yield only minor contributions to the correlation energy and have been neglected in the QMC treatment. A similar behavior can be found for the $^3P$ ground state of C. The contribution of the $2p^4$ occupation is only half as much as for the B atom, on the other hand it increases the importance of the $2s^1 2p^2 3d^1$ occupation slightly. The most important CSF besides HF of the $^4S$ ground state of N has a $2s^1 2p^3 3d^1$ occupation. Next to it there are three CSFs with $2s^1 3s^1 2p^2 3p^1$ occupation. Up to now there is a clear order of precedence for the contributions of different occupations. This is no longer valid for the ground states of O and F. For the $^3P$ state of O there are similar contributions from the $2s^1 2p^4 3d^1$,

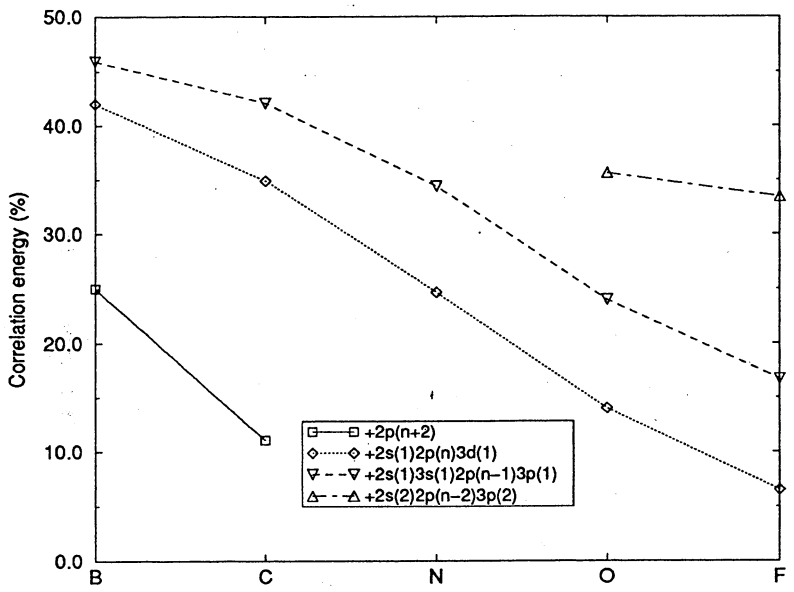


Figure 3: CASSCF calculations. Contributions of selected CSFs to the correlation energy of the atoms B to F. The groups of CSFs which belong to a given occupation have been added consecutively to the HF configuration. All CSFs which belong to a given occupation have been included.

$2s^1 3s^1 2p^3 3p^1$ and $2s^2 2p^2 3p^2$ configurations. The contribution of $2s^2 2p^n \rightarrow 2s^1 2p^n 3d^1$ excitations decreases significantly from N to O, whereas the $2s^2 2p^n \rightarrow 2s^2 2p^{n-2} 3p^2$ excitations come to the fore. The behavior of the $^2P$ ground state of F continues along this line. The CSFs with $2s^2 2p^3 3p^2$ occupation become dominant in this case.

## 4. Fixed-node PDMC calculations with different types of trial wave functions.

We have performed pure diffusion Monte Carlo (PDMC) calculations [5] within the fixed-node and short-time approximation for the atoms B to Ne. The PDMC method is based on a generalization of the Feynman-Kac formula for the imaginary time Green's function, which allows importance sampling with a given trial wave function.

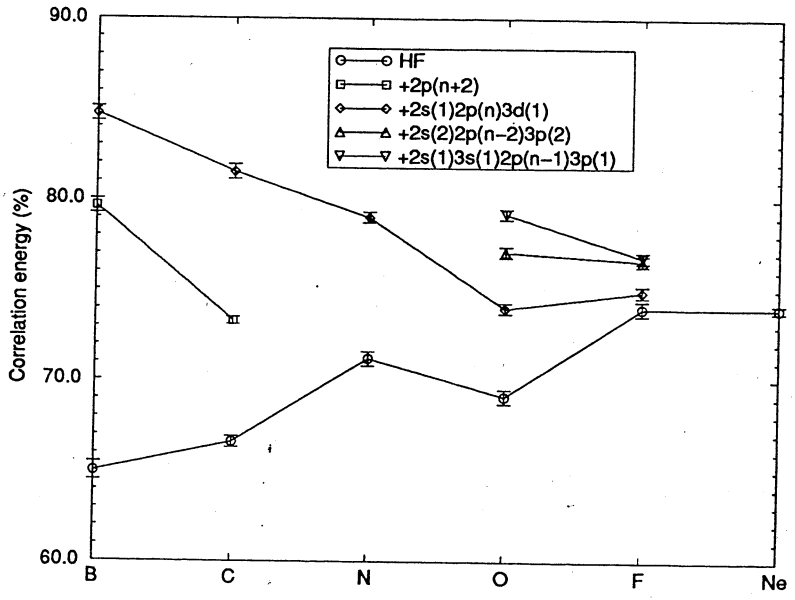


Figure 4: Variation of the percentage of the correlation energy for the atoms B to Ne in variational Monte Carlo (VMC) calculations. For each atom selected groups of CSFs which belong to a given occupation have been added consecutively to the HF configuration. The parameters of the Jastrow factors have been optimized for HF wave functions only and have been kept unchanged for the multi-reference wave functions.

The energy is calculated from the time-dependent equation

$$\frac{\langle \Psi \mid \hat{H} \exp\left(-\beta \hat{H}\right) \mid \Psi \rangle}{\langle \Psi \mid \exp\left(-\beta \hat{H}\right) \mid \Psi \rangle} = \lim_{T \to \infty} \frac{\int_0^T d\tau \frac{1}{2} \left(E_L(\vec{r}_\tau) + E_L(\vec{r}_{\tau+\beta})\right) \exp\left(-\int_\tau^{\tau+\beta} E_L(\vec{r}_s) ds\right)}{\int_0^T d\tau \exp\left(-\int_\tau^{\tau+\beta} E_L(\vec{r}_s) ds\right)} \tag{16}$$

with the local energy

$$E_L(\vec{r}) = \frac{\hat{H}\Psi(\vec{r})}{\Psi(\vec{r})} \tag{17}$$

calculated from the trial wave function $\Psi$. The right hand side represents a fraction of path integrals extending over all paths of length $\beta$ which can be generated by the stochastic differential equation

$$d\vec{x} = \frac{\nabla \Psi}{\Psi} d\tau + d\vec{W} \tag{18}$$

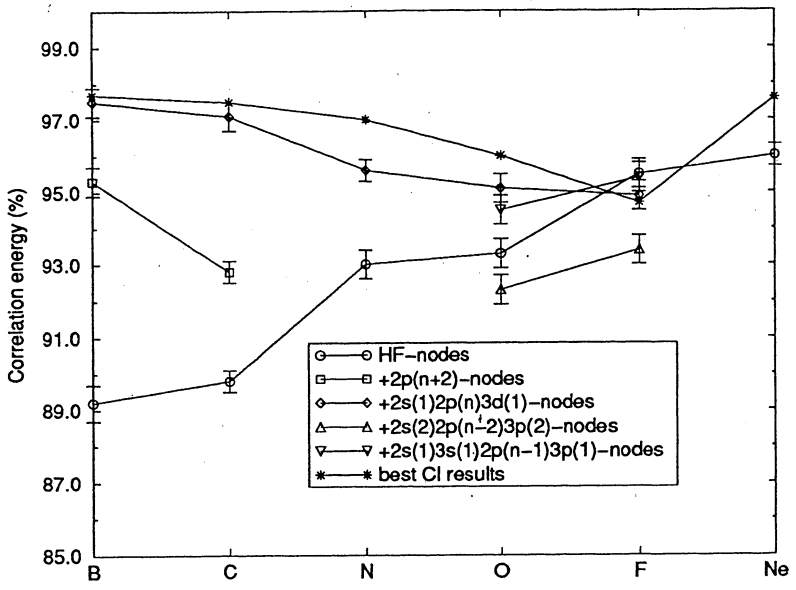


Figure 5: Variation of the percentage of the correlation energy for the atoms B to Ne in fixed-node pure diffusion Monte Carlo (PDMC) calculations. For each atom selected groups of CSFs which belong to a given occupation have been added consecutively to the HF configuration.

where $\vec{W}$ is a Wiener process. In the case of finite systems it is sufficient to generate one infinitely long path parameterized by $\tau$ and to subdivide it. For $\beta = 0$ we obtain the variational Monte Carlo (VMC) result, which means that we have calculated the energy expectation value for the trial wave function $\Psi$. In the limit $\beta \to \infty$ we get the exact ground state energy for the Schrödinger equation with imposed fixed-node boundary condition on the solution. It is imposed through Eq. (18) where the drift term keeps walkers away from the nodes. The resulting energy is an upper bound of the exact ground state energy. To generate a random walk by Eq. (18) it is necessary to choose a finite time step $\Delta\tau$. This leads to the so-called short-time error. The trial wave functions $\Psi$ are composed of a HF or multi-configuration wave function $\Phi$ and a Jastrow factor. Although we have considered only HF nodes for Ne, we will mention it below for the sake of completeness. We have chosen the following ansatz

for the Jastrow factor [29]

$$\Psi = \prod_{i<j} \exp\{U_G[U_{G0}(r_i, r_j), r_{ij}]\}\,\Phi \tag{19}$$

$$U_G = \frac{U_{G0} + c_1 r_{12}}{1 + [(c_1 - \frac{1}{2})/U_{G0}]r_{12} + c_2 r_{12}^2}$$

$$U_{G0}(r_i, r_j) = -\left[\frac{2}{3}\pi \sum_l d_l \left(\frac{\alpha_l}{\pi}\right)^{\frac{3}{2}} \left(e^{-\alpha_l r_i^2} + e^{-\alpha_l r_j^2}\right)\right]^{-\frac{1}{3}}$$

which contains the free parameters $c_1, c_2, \alpha_l, d_l$. They are optimized by minimizing the variance of the local energy [30] for a given number of points in configuration space. The points are distributed according to $\Psi^2$ for a given set of parameters and held fixed during the optimization. The whole procedure has been repeated for the new set of parameters until no further improvement could be achieved. The Jastrow factor has been described in more detail in ref. [29] which also contains a list of parameters for the atoms discussed below. The parameters have been optimized only for $\Phi$ taken from HF calculations. This is sufficient for our purposes because Jastrow factors do not change the nodes. Furthermore Jastrow factors are especially intended for the description of short-range correlations, whereas the MCSCF parts describe mainly near-degeneracies. At least in a first approximation it can be assumed that they act independently on the electrons. We will discuss this point subsequently. In order to study the influence of the short-time approximation on our results, we have performed calculations with HF trial wave functions for various values of the time step. The chosen time steps are small enough to get no significant dependence of our results on their magnitudes. This has been confirmed by a comparison of our results with domain Green's function Monte Carlo (DGFMC) calculations of Subramaniam *et al.* [31] as will be discussed below.

Before we enter into the discussion of the PDMC calculations we will briefly consider the VMC energies for the various trial wave functions. The VMC energies have been plotted in Figure 4 corresponding to the CASSCF energies in Figure 3. The differences in the correlation energies between both figures are due to the Jastrow factors with which the multi-configuration wave functions have been multiplied. Comparing Figures 3 and 4 it is clear that the relative energy differences between the wave functions decrease in going from B to F. In the case of F the energy difference amounts only 3 % in VMC compared with 33 % in CASSCF calculations. This indicates, that the additional CSFs and the Jastrow factors describe similar parts of electron correlation. On the other side a more complementary behavior can be observed for B and C.

The fixed-node PDMC energies for the various trial wave functions discussed above are presented in Figure 5 and Table 1. It can be seen, that PDMC and VMC behave rather similar along the row B to Ne. The HF nodes turn out to be a very poor approximation for B and C. Only 89.2(5) % and 89.8(3) %, respectively, have

been recovered for these atoms. Taking care of the $2s^2 2p^n \rightarrow 2p^{n+2}$ near-degeneracy improves the results to 95.3(4) % and 92.8(3) %, respectively, which is equivalent to the Be atom discussed above. Moreover improvements can be achieved by adding further all CSFs belonging to a $2s^1 2p^n 3d^1$ occupation. For our best trial wave functions 97.5(4) % and 97.1(4) % of the correlation energy is recovered for B and C. For the atoms N, O and F the HF fixed-node energies recover 93.0(4) % to 95.5(4) % of the correlation energy. The HF nodes become more reasonable in going from B to F. Adding the CSFs which belong to a $2s^1 2p^n 3d^1$ occupation improves the correlation energy to 95.6(3) % and 95.1(4) % for N and O, but leaves F nearly unchanged. This agrees well with the CASSCF calculations, which show that these CSFs are only of minor importance for F. The CASSCF results of Figure 3 indicate that for O and F other configurations become more important. These are CSFs with $2s^2 2p^{n-2} 3p^2$ and $2s^1 3s^1 2p^{n-1} 3p^1$ occupations. In the case of O we obtained from the CASSCF calculations $2s^2 2p^2 3p^2$ as the most important occupation for additional CSFs. We have first added only CSFs which belong to this occupation to the HF configuration and obtained only 91.2(4) % (see Table 2) of the correlation energy. This is an example of a decreasing PDMC correlation energy with simultaneous increase of the corresponding VMC value. Adding the $2s^1 2p^4 3d^1$ and $2s^2 2p^2 3p^2$ configurations we get 92.3(4) % which is still a little below the PDMC result with HF nodes. The correlation energy can be further improved by including the extra CSFs belonging to $2s^1 3s^1 2p^3 3p^1$. The resulting 94.5(4) % corresponds to our result obtained by taking into account only the $2s^1 2p^4 3d^1$ configurations. For F the results are even more discouraging. In the CASSCF calculations $2p^5 \rightarrow 2p^3 3p^2$ excitations give the chief contribution but the PDMC correlation energy decreases to 92.5(4) % after expanding the HF wave function by the CSFs belonging to it. If we add instead of these CSFs all that belong to the $2s^1 3s^1 2p^4 3p^1$ occupation, the correlation energy becomes even worse, only 91.0(4) % is recovered in this PDMC calculation. However if we add all CSFs to the HF configuration which belong to $2s^1 2p^5 3d^1$, $2s^2 2p^3 3p^2$, $2s^1 3s^1 2p^4 3p^1$ occupations we get again 95.4(4) % of the correlation energy.

These results indicate, that an improvement of the nodal structure is not equivalent to an improvement of the correlation energy of the multi-reference wave function. Some indications can be obtained from VMC calculations. If Jastrow factor and multi-reference wave function complement each other, it can be expected that the nodes improve with respect to HF. This type of behavior is mainly observed in cases where near-degeneracies occur like for B and C. For atoms like O and F the situation is more complicated. A significant deterioration of the results can be obtained by adding only a restricted set of CSFs as can be seen in Table 2. It seems to be important to include all CSFs which yield comparable contributions to the correlation energy and to avoid an arbitrary selection. In order to proceed along this line, it is necessary to get a better understanding how CSFs influence the nodes. An interesting question is the occurrence of spurious nodes. Is it possible to change the topology of the nodal hypersurface by adding particular CSFs or do they merely generate deformations?

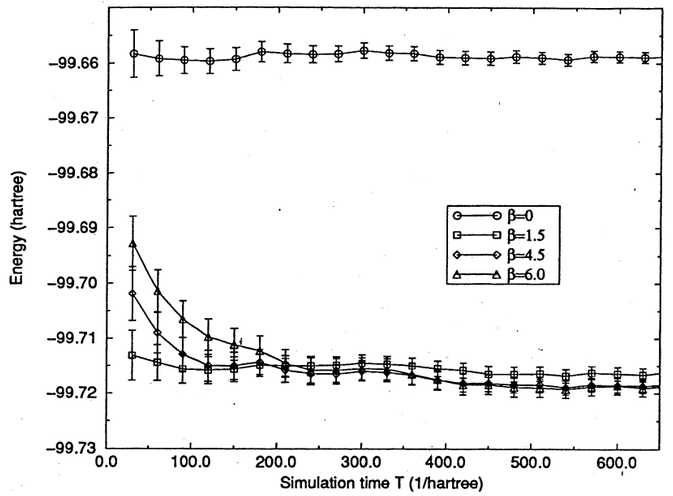


Figure 6: Energy evolution during a simulation of the F atom for different values of $\beta$.

This will be a subject of further studies.

## 5. Computational details.

We have generated the coupling schemes for our wave functions using the program GENCL [24] of Froese Fischer. The CI coefficients belonging to the different CSFs have been obtained using the atomic MCHF program [24] of Froese Fischer.

The procedure discussed above for the generation of spin-free trial wave functions has been implemented in our QMC program. In order to check the reliability of our program we have performed some independent tests on the resulting trial wave functions. A simple check can be performed using a molecular MCSCF program. These programs do not take account of the full atomic symmetries but it is possible to perform a state-averaged CASSCF calculation in a determinant basis. Comparing the absolute values of the coefficients of the determinants with those in the spin-free case provides an easy check, which can be used to verify the signs of the coefficients of the CSFs. We have used the MOLPRO program of Werner and Knowles [25, 26] for this purpose. The ultimate test is to perform a VMC calculation and to compare the

energy with the MCHF result. Although the statistical errors are quite large in VMC calculations without Jastrow factors, it is possible to get sufficient accuracy to have a sensitive test of the trial wave function. We have used nodeless Slater type orbitals (STOs) basis functions to represent the radial parts of the orbitals. The (6s,4p) STO basis sets of Clementi and Roetti [33] which we have employed in our calculations are close to the HF limit and are sufficiently flexible to represent 3s- and 3p-orbitals. For the HF trial wave functions the coefficients of the STOs can be taken from [33]. In the multi-reference case we have used a STO-6G expansion [34, 35] where each STO is represented by a linear combination of 6 Gaussian type orbitals (GTOs). This enables the calculation of the orbitals with the MCSCF part of MOLPRO. We have checked the accuracy of this procedure for F by comparing VMC and PDMC energies obtained with orbitals from the STO-6G expansion and those from Clementi and Roetti. The 3d-orbitals are represented by a single STO with optimized exponents 1.500, 1.825, 2.174, 2.695, 3.173 for B, C, N, O and F. This has been shown to be sufficiently accurate for our purposes.

As mentioned above our PDMC calculations are based on the short-time approximation. Taking into account detailed balance in each step of the simulation together with good trial wave functions reduce the short-time error below the statistical uncertainty for appropriately chosen time steps. We have taken time steps of 0.005, 0.005, 0.004, 0.004, 0.003 $hartree^{-1}$ for B, C, N, O and F. In order to check the short-time approximation we have also performed PDMC calculations for each element taking time steps larger by 0.003 $hartree^{-1}$. The results agree within the statistical uncertainties. Therefore it is to be supposed that our results are not significantly biased by the short-time approximation. In all simulations we have sampled 200 independent values for the energy from which we have calculated the standard deviation of the mean energy.

In PDMC calculations it is necessary to consider $lim_{T\to\infty}$ and $lim_{\beta\to\infty}$ as can be seen from equation (16). We have checked the convergence with respect to both parameters by considering the evolution of a series of different values for $\beta$. In Figure 6 we have plotted the behavior of different $\beta$ during the simulation. In the following all times refer to $hartree^{-1}$. For $\beta = 0$ we observe statistical fluctuations which decrease with increasing simulation time. At $\beta = 1.5$ we get a large decrease in energy relative to $\beta = 0$, which remains constant apart from statistical fluctuations. For $\beta = 4.5$ a rapid decrease in energy has been observed for small values of T. After a total simulation time T of app. 250 $hartree^{-1}$ the energy remains constant and below the value for $\beta = 1.5$. The same behavior can be observed for $\beta = 6.0$, except from the increasing simulation time which is necessary to achieve a constant energy. This can be explained by statistical dependencies at the beginning of the walk. Let us assume, that we have performed enough steps to generate one path of length $\beta$, which will contribute with a weight

$$\exp\left(-\int_0^\beta E_L(\vec{r}_s)ds\right) \tag{20}$$

in the path integral. After performing the next step $\Delta\tau$ we can add the next path with weight

$$\exp\left(-\int_{\Delta\tau}^{\beta+\Delta\tau} E_L(\vec{r}_s)ds\right) \tag{21}$$

It is clear, that the second path is nearly identical to the first one and therefore both will nearly have the same weight. The same will be true for the following N steps until we have $N\Delta\tau > \beta$. At the beginning of our simulation we sum only over statistically highly dependent paths. This means that the weight factor in equation (16) is approximately constant and can be factored out in both the numerator and denominator. As a result we obtain approximately a sum over $E_L$s which are distributed according to $\Psi^2$ yielding the VMC energy. If we continue the simulation we obtain independent paths and the energy decreases until we have a representative selection of statistically independent paths. From that point on we observe no systematic variations in the energy. The number of steps which are necessary to reach this point clearly depends on the magnitude of $\beta$, which can be seen in Figure 6. The convergence with respect to $\beta$ is very fast, so that we can extract the final energy without problems.

## 6. Comparison with previous QMC and other *ab initio* calculations.

In the following we will compare our results with quantum Monte Carlo calculations reported in the literature. We will consider the percentage of the total correlation energy obtained in the various calculations. We have referred all results to the estimated exact nonrelativistic correlation energies of Davidson *et al.* [32]. Statistical errors in the last digit are given in parentheses.

For the B atom a DGFMC calculation with HF-nodes, yielding 91(3) % [31] was the only one published to our knowledge. This agrees within the statistical error with our result of 89.2(5) %. In the case of the C atom DGFMC yields 89(8) % [31]. GFMC calculations of Schmidt and Moskowitz yield 89(3) %, 98(3) % with HF-, MCSCF-nodes [36]. Unfortunately they did not specify the selected configurations. Our results of 89.8(3) % and 97.1(4) %, respectively, are in close agreement with these calculations. For N we can compare with a DMC calculation of Reynolds *et al.* [37]. They obtained 93.2(6) % with HF-nodes in comparison to our calculation which yields 93.0(4) %. The DGFMC calculation of Subramaniam *et al.* yielded 97(10) % for the O atom compared to our value of 93.3(4) % obtained with HF-nodes. There are two significantly different values for the F atom reported in the literature. Reynolds *et al.* obtained 89.8(6) % [37] whereas Garmer and Anderson [38] got 95.1(2) % of the total correlation energy. Both calculations are based on HF-nodes but Garmer and Anderson used the better basis set. We obtained a similar result to that of Garmer and Anderson, namely 95.5(4) %. Finally, we will mention the Ne atom, where Umrigar *et al.* obtained 96(1) % [39] which is also in perfect agreement with our result of 96(1) %.

To see how our correlation energies fit into the results of other *ab initio* methods we have mentioned the most accurate configuration interaction (CI) calculations for these atoms reported in the literature (for a review see e.g. [40]). In Table 3 we have compared these results with our best PDMC calculations. The percentages of the total correlation energies have been calculated with respect to the experimental values of Davidson *et al.* [32]. Our first reference is the classical work of Sasaki and Yoshimine [41] which has been slightly improved by the work of Feller and Davidson [42]. The CI treatment in [41] includes selected single, double, triple and quadruple excitations and is based on a very large STO basis set including up to i-orbitals. Feller and Davidson [42] used the multi-reference CI method and large GTO type basis sets including up to g-orbitals. Only selected CSFs were included in the calculations. Their results are probably at present the best available correlation energies for these atoms, obtained with a strictly variational method. We have also included some coupled-cluster (CCSD(T)) calculations which yield some further improvement with respect to the MRCI results of Feller and Davidson. The triple excitations have been treated by perturbation theory. Although CC methods are not strictly variational, they usually give highly reliable correlation energies.

It can be seen, that fixed-node PDMC calculations can compete with these methods if the nodes are improved beyond HF by adding further CSFs. Unfortunately, it is not easily possible to decide which CSFs are important for the nodes. In some cases the results become even worse after adding additional CSFs. This is in contrast to CI methods, where the addition of further CSFs or the expansion of the basis set can only improve the correlation energy.

## Acknowledgment.

The authors are grateful to the "Institut du Développement et des Ressources en Informatique Scientifique" (IDRIS-CNRS, Orsay France) for providing them with computer time.

## Appendix A. Coupling schemes for the CSFs used in QMC calculations.

We have listed in this appendix all CSFs that have been used in the PDMC calculations. The CSFs are characterized by their coupling scheme, which has been generated using the GENCL program of Froese Fischer [24]. The contributions of closed shells have been omitted. Open shells $l^n$ with $n \geq 3$ are in general not uniquely characterized by their $L, S$ values. It is necessary to specify in addition the seniority number $\sigma$ [23], which depends on the number $n_p$ of electron pairs coupled to zero angular momentum. It is defined by $\sigma = n - 2n_p$ and is placed on the lower left part of the term symbol $({}^{2S+1}_{\sigma}L)$.

Table 1: Fixed-node pure diffusion Monte Carlo (PDMC) and variational Monte Carlo (VMC) energies (*hartree*) for various types of trial wave functions. Statistical errors on the last digit are given in parentheses. The last column gives the number of determinants of the trial wave function.

| Nodes | PDMC | % | VMC | % | Determinants |
|---|---|---|---|---|---|
| B $^2P$ | | | | | |
| Hartree Fock | -24.6404 (7) | 89.2 (5) | -24.6102 (6) | 65.0 (5) | 1 |
| $+2p^3$ | -24.6480 (5) | 95.3 (4) | -24.6284 (5) | 79.6 (4) | 3 |
| $+2s^12p^13d^1$ | -24.6508 (5) | 97.5 (4) | -24.6348 (4) | 84.7 (4) | 12 |
| Exact energy[a] | -24.65393 | | | | |
| C $^3P$ | | | | | |
| Hartree Fock | -37.8291 (5) | 89.8 (3) | -37.7928 (5) | 66.6 (3) | 1 |
| $+2p^4$ | -37.8338 (4) | 92.8 (3) | -37.8032 (3) | 73.3 (2) | 2 |
| $+2s^12p^23d^1$ | -37.8404 (7) | 97.1 (4) | -37.8159 (7) | 81.4 (4) | 18 |
| Exact energy | -37.8450 | | | | |
| N $^4S$ | | | | | |
| Hartree Fock | -54.5760 (8) | 93.0 (4) | -54.5359 (7) | 71.7 (4) | 1 |
| $+2s^12p^33d^1$ | -54.5810 (6) | 95.6 (3) | -54.5497 (6) | 79.0 (3) | 12 |
| Exact energy | -54.5893 | | | | |
| O $^3P$ | | | | | |
| Hartree Fock | -75.0498 (10) | 93.3 (4) | -74.9875 (9) | 69.1 (4) | 1 |
| $+2s^12p^43d^1$ | -75.0546 (9) | 95.1 (4) | -75.0002 (7) | 74.0 (3) | 17 |
| $+2s^22p^23p^2$ | -75.0474 (9) | 92.3 (4) | -75.0082 (8) | 77.1 (3) | 31 |
| $+2s^13s^12p^33p^1$ | -75.0530 (9) | 94.5 (4) | -75.0137 (8) | 79.2 (3) | 62 |
| Exact energy | -75.067 | | | | |
| F $^2P$ | | | | | |
| Hartree Fock | -99.7190 (14) | 95.5 (4) | -99.6493 (12) | 74.0 (4) | 1 |
| $+2s^12p^53d^1$ | -99.7171 (12) | 94.9 (4) | -99.6524 (11) | 74.9 (3) | 10 |
| $+2s^22p^33p^2$ | -99.7121 (10) | 93.3 (3) | -99.6578 (8) | 76.6 (3) | 38 |
| $+2s^13s^12p^43p^1$ | -99.7187 (14) | 95.4 (4) | -99.6586 (9) | 76.8 (3) | 67 |
| Exact energy | -99.734 | | | | |

[a] The exact energies have been taken from [32].

Table 2: Fixed-node pure diffusion Monte Carlo (PDMC) and variational Monte Carlo (VMC) energies (*hartree*) for CSFs belonging to the specified occupations, which lead to a deterioration with respect to HF nodes if added separately to the HF configuration. Statistical errors on the last digit are given in parentheses.

| Atom | Nodes | PDMC | % | VMC | % |
|---|---|---|---|---|---|
| O | $2s^2 2p^2 3p^2$ | -75.0445 (9) | 91.2 (4) | -74.9949 (8) | 72.0 (3) |
| F | $2s^2 2p^3 3p^2$ | -99.7094 (12) | 92.5 (4) | -99.6511 (10) | 74.5 (3) |
| F | $2s^1 3s^1 2p^4 3p^1$ | -99.7044 (12) | 91.0 (4) | -99.6423 (13) | 71.8 (4) |

Table 3: Comparison of fixed-node PDMC correlation energies with MRCI and CCSD(T) results reported in the literature. Statistical errors on the last digit are given in parenthesis.

| Method | Reference | B | C | N | O | F |
|---|---|---|---|---|---|---|
| CI(SDTQ) | [41] | 96.8 | 96.4 | 95.7 | 95.0 | 94.7 |
| MRCI | [42] | 97.7 | 97.5 | 97.0 | 95.8 [a] | 94.6 |
| CCSD(T) | [44] | | | | | 95.6 |
| CCSD(T) | [45] | | | | 96.7 | |
| PDMC | Present work | 97.5(4) | 97.1(4) | 95.6(3) | 95.1(4) | 95.5(4) |

[a] A slightly improved result (96.0) is reported in ref. [43].

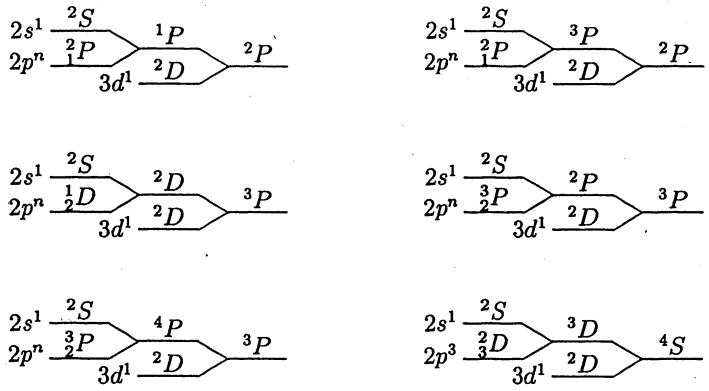


Figure 7: Coupling schemes for CSFs with a $2s^1 2p^n 3d^1$ occupation. The first two diagrams represent CSFs belonging to the $^2P$ states of B and F, followed by three diagrams for the $^3P$ states of C and O. The last diagram represents the CSF for the $^4S$ state of N.

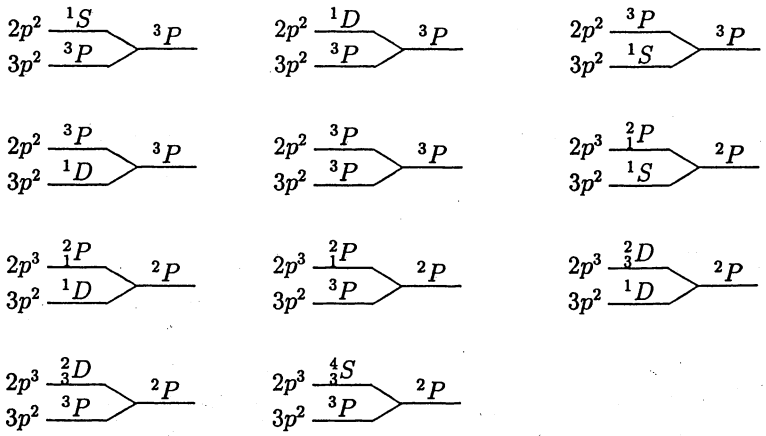


Figure 8: Coupling schemes for CSFs with a $2s^2 2p^{n-2} 3p^2$ occupation. The first five diagrams represent CSFs belonging to the $^3P$ state of O, followed by six diagrams for the $^2P$ state of F.

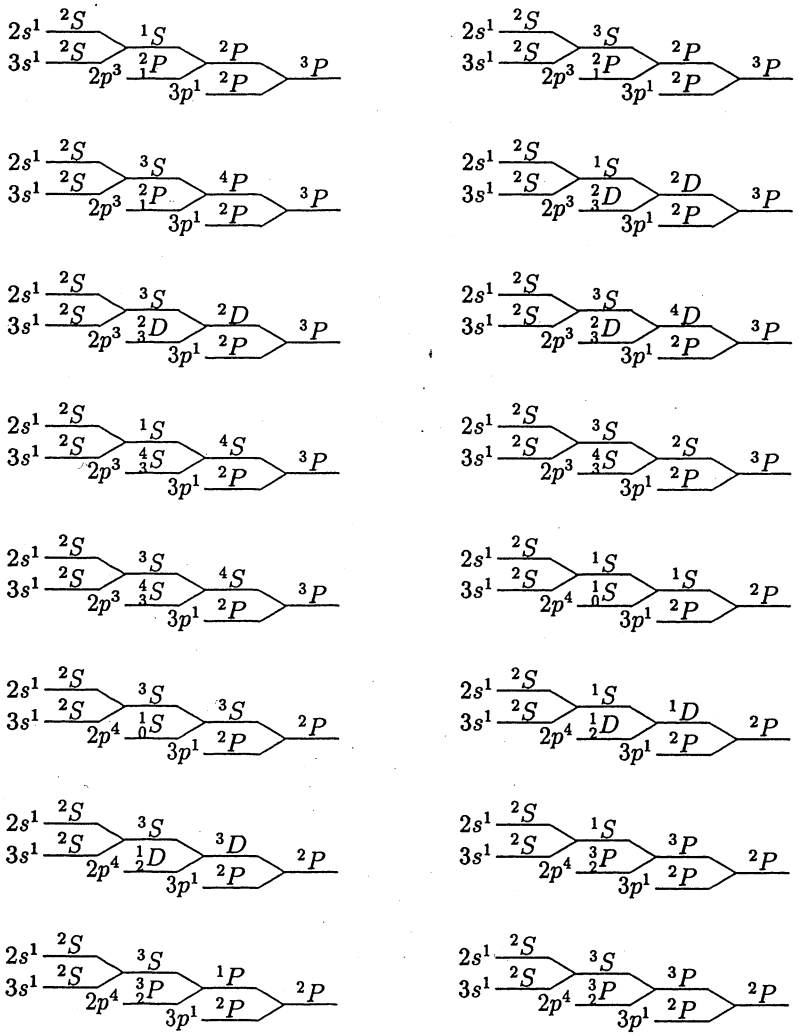


Figure 9: Coupling schemes for CSFs with a $2s^1 3s^1 2p^{n-1} 3p^1$ occupation. The first nine diagrams represent CSFs belonging to the $^3P$ state of O, followed by seven diagrams for the $^2P$ state of F.

## Appendix B. The explicit construction of spin-free CSFs.

In this appendix we consider a simple example for the construction of spin-free CSFs in detail. For the $^2P$ state of the B atom we have two CSFs which belong to the $2s^1 2p^1 3d^1$ occupation (see Figure 7). The angular momentum eigenfunction $\phi_{10}$ is obtained by coupling the 2p- and 3d-shell.

$$\begin{aligned}\phi_{10}(1,2) &= \sqrt{\frac{3}{10}}\,\{Y_{1(-1)}(1)\,Y_{21}(2) + Y_{11}(1)\,Y_{2(-1)}(2)\} \\ &- \sqrt{\frac{2}{5}}\,Y_{10}(1)\,Y_{20}(2) \qquad (22)\end{aligned}$$

After inserting real spherical harmonics and multiplying with the 2s-orbital we get

$$\begin{aligned}\phi_{10}(1,2,3) &= \sqrt{\frac{3}{10}}\,\{2p_x(1)\,3d_{xz}(2)\,2s(3) + 2p_y(1)\,3d_{yz}(2)\,2s(3)\} \\ &+ \sqrt{\frac{2}{5}}\,2p_z(1)\,3d_{z^2-r^2}(2)\,2s(3) \qquad (23)\end{aligned}$$

using the commonly adopted notation for the real orbitals in the 2p- and 3d-shell. Figure 10 shows the two possible standard Young tableaux. If we apply $\hat{E}_{Y_1}$ to $\phi_{10}$ (see Eq. 6) we obtain the first CSF.

$$\begin{aligned}\Phi_1(1,2,3) &= \sqrt{\frac{3}{10}}\{|2s(1)\,2p_x(3)|\,3d_{xz}(2) + |2s(1)\,3d_{xz}(3)|\,2p_x(2)\} \\ &+ \sqrt{\frac{3}{10}}\{|2s(1)\,2p_y(3)|\,3d_{yz}(2) + |2s(1)\,3d_{yz}(3)|\,2p_y(2)\} \\ &+ \sqrt{\frac{2}{5}}\{|2s(1)\,2p_z(3)|\,3d_{z^2-r^2}(2) + |2s(1)\,3d_{z^2-r^2}(3)|\,2p_z(2)\} \qquad (24)\end{aligned}$$

The second Young tableau can be obtained from the first by interchanging 2 and 3. Therefore if we interchange the two variables in Eq. 23 and apply again $\hat{E}_{Y_1}$ we obtain the second possible CSF.

$$\begin{aligned}\Phi_2(1,2,3) &= \sqrt{\frac{3}{10}}\{|2p_x(1)\,3d_{xz}(3)|\,2s(2) + |2s(1)\,3d_{xz}(3)|\,2p_x(2)\} \\ &+ \sqrt{\frac{3}{10}}\{|2p_y(1)\,3d_{yz}(3)|\,2s(2) + |2s(1)\,3d_{yz}(3)|\,2p_y(2)\} \\ &+ \sqrt{\frac{2}{5}}\{|2s(1)\,3d_{z^2-r^2}(3)|\,2p_z(2) + |p_z(1)\,3d_{z^2-r^2}(3)|\,2s(2)\} \qquad (25)\end{aligned}$$

In the first two coupling schemes in Figure 7 the 2s- and 2p-orbitals are coupled to a singlet and a triplet state, respectively. By inspection of Eq. 24 we see that the


Figure 10: Standard Young tableaux for the $^2P$ state of the B atom.

first, third and fifth terms contain both 2s- and 2p-orbitals in the determinant. As a consequence these terms belong to triplet coupling and cannot occur in the singlet case. Therefore it is only necessary to orthogonalize $\Phi_1$ with respect to $\Phi_2$ to obtain the desired CSFs.

$$\begin{aligned} \overline{\Phi}_1(1,2,3) &= \frac{1}{\sqrt{6}}\{2\,\Phi_1(1,2,3) - \Phi_2(1,2,3)\} \\ \overline{\Phi}_2(1,2,3) &= \frac{1}{\sqrt{2}}\,\Phi_2(1,2,3) \end{aligned} \tag{26}$$

The assignment is unique because every rotation of the $\overline{\Phi}_i$ leads inevitably to the occurrence of triplet terms in both CSFs.

We will close this appendix by constructing the antisymmetric spin-dependent wave function given in Eq. 7. Interchanging rows and columns transforms $Y_1$ to $Y_2$. If we apply the operator $\hat{P}_{Y_2}\hat{N}_{Y_2}$ to the primitive spin function $\alpha(1)\beta(2)\alpha(3)$ we get

$$\Xi_1(1,2,3) = 2\,\alpha(1)\beta(2)\alpha(3) - \alpha(2)\,\{\alpha(1)\beta(3) + \beta(1)\alpha(3)\} \tag{27}$$

Neglecting the normalization constant we obtain from Eq. 7

$$\begin{aligned} \Psi_1[(\vec{r}\vec{\sigma})_1, (\vec{r}\vec{\sigma})_2, (\vec{r}\vec{\sigma})_3] &= \Phi_1(\vec{r}_1,\vec{r}_2,\vec{r}_3)\,\Xi_1(\vec{\sigma}_1,\vec{\sigma}_2,\vec{\sigma}_3) \\ &- \Phi_1(\vec{r}_1,\vec{r}_3,\vec{r}_2)\,\Xi_1(\vec{\sigma}_1,\vec{\sigma}_3,\vec{\sigma}_2) \\ &+ \Phi_1(\vec{r}_2,\vec{r}_3,\vec{r}_1)\,\Xi_1(\vec{\sigma}_2,\vec{\sigma}_3,\vec{\sigma}_1) \end{aligned} \tag{28}$$

which can be rewritten into the more familiar linear combination of determinants.

$$\begin{aligned} \Psi_1(1,2,3) &= \sqrt{\frac{3}{10}}\{|2s^\alpha(1)\,2p_x^\beta(2)\,3d_{xz}^\alpha(3)| - |2s^\alpha(1)\,2p_x^\alpha(2)\,3d_{xz}^\beta(3)|\} \\ &+ \sqrt{\frac{3}{10}}\{|2s^\alpha(1)\,2p_y^\beta(2)\,3d_{yz}^\alpha(3)| - |2s^\alpha(1)\,2p_y^\alpha(2)\,3d_{yz}^\beta(3)|\} \\ &+ \sqrt{\frac{2}{5}}\{|2s^\alpha(1)\,2p_z^\beta(2)\,3d_{z^2-r^2}^\alpha(3)| - |2s^\alpha(1)\,2p_z^\alpha(2)\,3d_{z^2-r^2}^\beta(3)|\} \end{aligned} \tag{29}$$

A similar expression can be obtained for $\Psi_2(1,2,3)$.

## References


[1] B. L. Hammond, W. A. Lester, Jr., and P. J. Reynolds, *Monte Carlo Methods in Ab Initio Quantum Chemistry* (World Scientific, Singapore, 1994).

[2] D. M. Arnow, M. H. Kalos, M. A. Lee and K. E. Schmidt, *J. Chem. Phys.* **77** (1982) 5562.

[3] S. Zhang and M. H. Kalos, *Phys. Rev. Lett.* **67** (1991) 3074.

[4] D. M. Ceperley and B. J. Alder, *J. Chem. Phys.* **81** (1984) 5833.

[5] M. Caffarel and P. Claverie, *J. Chem. Phys.* **88** (1988) 1088; ibid. 1100.

[6] J. B. Anderson, C. A. Traynor and B. M. Boghosian, *J. Chem. Phys.* **95** (1991) 7418; see also, J. B. Anderson, *J. Chem. Phys.* **96** (1992) 3702.

[7] J. B. Anderson, *J. Chem. Phys.* **63** (1975) 1499; *ibid* **65** (1976) 4121.

[8] J. B. Anderson, *Int. Rev. Phys. Chem.* **14** (1995) 85.

[9] P. A. Christiansen, *J. Chem. Phys.* **95** (1991) 361.

[10] L. Mitáš, in *Computer Simulation Studies in Condensed Matter Physics V*, eds. D. P. Landau, K. K. Mon and H. B. Schüttler (Springer-Verlag, Berlin, 1993) p.94.

[11] L. Mitáš, *Phys. Rev. A* **49** (1994) 4411.

[12] H.-J. Flad and M. Dolg, *Ground state properties of $Hg_2$. II. A quantum Monte Carlo study.* Accepted by J. Phys. Chem.

[13] D. M. Ceperley, *J. Stat. Phys.* **63** (1991) 1237.

[14] D. J. Klein and H. M. Pickett, *J. Chem. Phys.* **64** (1976) 4811.

[15] R. J. Harrison and N. C. Handy, *Chem. Phys. Lett.* **113** (1985) 257.

[16] J. C. Grossman and L. Mitas, *Phys. Rev. Lett.* **74** (1995) 1323.

[17] R. Pauncz, *Spin Eigenfunctions* (Plenum Press, New York, 1979)

[18] L. D. Landau and E. M. Lifschitz, *Quantum Mechanics* (Pergamon Press, Oxford, 1958).

[19] V. Fock, *Izv. Akad. Nauk. SSSR, Ser. Fiz.* **18** (1954) 161.

[20] M. Hamermesh, *Group Theory and its Application to Physical Problems* (Addison-Wessley, Reading Mass., 1962).

[21] G. F. Drukarev, *Soviet Phys. JETP* **4**, 309 (1957).

[22] I. N. Demkov, *Soviet Phys. JETP* **34**, 491 (1958).

[23] I. Lindgren and J. Morrison, *Atomic Many-Body Theory* (Springer-Verlag, Berlin, 1982)

[24] C. Froese Fischer, *Comput. Phys. Commun.* **64**, 369 (1991).

[25] MOLPRO is a package of *ab initio* programs written by H.-J. Werner and P.J. Knowles, with contributions from J. Almlöf, R.D. Amos, M.J.O. Deegan, S.T. Elbert, C. Hampel, W. Meyer, K. Peterson, R.M. Pitzer, A.J. Stone, and P.R. Taylor.

[26] H.-J. Werner and P. J. Knowles, *J. Chem. Phys.* **82** (1985) 5053; P. J. Knowles and H.-J. Werner, *Chem. Phys. Lett.* **115** (1985) 259.

[27] I. Shavitt, in *Methods of Electronic Structure Theory*, ed. H. F. Schaefer III (Plenum Press, New York, 1977) p. 189.

[28] W. Kutzelnigg, *Theor Chim Acta* **68** (1985) 445.

[29] H.-J. Flad and A. Savin *J. Chem. Phys.* **103** (1995) 691.

[30] C. J. Umrigar, K. G. Wilson and J. W. Wilkins *Phys. Rev. Lett.* **60** (1988) 1719.

[31] R. P. Subramaniam, M. A. Lee, K. E. Schmidt and J. W. Moskowitz, *J. Chem. Phys.* **97** (1992) 2600.

[32] E. R. Davidson, S. A. Hagstrom, S. J. Chakravorty, V. Meiser Umar and C. Froese Fischer, *Phys. Rev. A* **44** (1991) 7071.

[33] E. Clementi and C. Roetti, *Atomic Data and Nuclear Data Tables* **14** (1974) 177.

[34] W. J. Hehre, R. F. Stewart and J. A. Pople, *J. Chem. Phys.* **51** (1969) 2657.

[35] W. J. Pietro, B. A. Levi, W. J. Hehre and R. F. Stewart, *Inorg. Chem.* **19** (1980) 2225.

[36] K.E. Schmidt and J.W. Moskowitz, *J. Stat. Phys.* **43** (1986) 1027.

[37] P. J. Reynolds, R. N. Barnett, B. L. Hammond and W. A. Lester,Jr., *J. Stat. Phys.* **43** (1986) 1017.

[38] D. R. Garmer and J. B. Anderson, *J. Chem. Phys.* **89** (1988) 3050.

[39] C. J. Umrigar, M. P. Nightingale and K. J. Runge, *J. Chem. Phys.* **99** (1993) 2865.

[40] M. Urban, R. J. Bartlett and S. A. Alexander, *Int. J. Quant. Chem. Symp.* **26** (1992) 271.

[41] F. Sasaki and M. Yoshimine, *Phys. Rev. A* **9** (1974) 17.

[42] D. Feller and E. R. Davidson, *J. Chem. Phys.* **88** (1988) 7580.

[43] D. Feller and E. R. Davidson, *J. Chem. Phys.* **90** (1989) 1024.

[44] G. E. Scuseria, *J. Chem. Phys.* **95** (1991) 7426.

[45] D. L. Strout and G. E. Scuseria, *J. Chem. Phys.* **96** (1992) 9025.